Vibrational and rotational CARS measurements of nitrogen in afterglow of streamer discharge in atmospheric pressure fuel/air mixtures

2012 J. Phys. D: Appl. Phys. 45 495401

(http://iopscience.iop.org/0022-3727/45/49/495401)

Report Documentation Page

Form Approved
OMB No. 0704-0188

1. REPORT DATE	2. REPORT TYPE	3. DATES COVERED
2012		**00-00-2012 to 00-00-2012**

4. TITLE AND SUBTITLE
Vibrational and rotational CARS measurements of nitrogen in afterglow of streamer discharge in atmospheric pressure fuel/air mixtures

5a. CONTRACT NUMBER
5b. GRANT NUMBER
5c. PROGRAM ELEMENT NUMBER

6. AUTHOR(S)

5d. PROJECT NUMBER
5e. TASK NUMBER
5f. WORK UNIT NUMBER

7. PERFORMING ORGANIZATION NAME(S) AND ADDRESS(ES)
Air Force Research Laboratory,Wright-Patterson Air Force Base,OH,45433

8. PERFORMING ORGANIZATION REPORT NUMBER

9. SPONSORING/MONITORING AGENCY NAME(S) AND ADDRESS(ES)

10. SPONSOR/MONITOR'S ACRONYM(S)
11. SPONSOR/MONITOR'S REPORT NUMBER(S)

12. DISTRIBUTION/AVAILABILITY STATEMENT
Approved for public release; distribution unlimited

13. SUPPLEMENTARY NOTES
J. Phys. D: Appl. Phys. 45 (2012) 495401 (8pp)

14. ABSTRACT
The use of nonequilibrium plasma generated by nanosecond discharges to ignite fuel/air mixtures, known as transient plasma ignition (TPI), has been shown to effectively reduce ignition delay and improve engine performance relative to spark ignition for combustion engines. While this method is potentially useful for many engine applications, at present the underlying physics are poorly understood. This work uses coherent anti-Stokes Raman spectroscopy (CARS) to measure the rotational and vibrational excitation of nitrogen molecules in the discharge afterglow in a variety of fuel/air mixtures outside the limits of combustion in order to elucidate the thermal behaviour of TPI. The time evolution of relative populations of vibrationally excited states of nitrogen in the electronic ground state are reported for each gas mixture; it is shown that generation of these vibrationally excited states is inefficient during the discharge in air but that generation occurs at a high rate roughly 5μs following the discharge; with the addition of fuels vibrationally excited states are observed during the discharge but an increase in population is still seen at 5μs. Possible mechanisms for this behaviour are discussed. In addition, rotational temperature increases of at least 500K are reported for all gas mixtures. The effect of this temperature increase on ignition, reaction rates, and thermal energy pathways are discussed

15. SUBJECT TERMS

16. SECURITY CLASSIFICATION OF:			17. LIMITATION OF ABSTRACT	18. NUMBER OF PAGES	19a. NAME OF RESPONSIBLE PERSON
a. REPORT	b. ABSTRACT	c. THIS PAGE			
unclassified	**unclassified**	**unclassified**	**Same as Report (SAR)**	**10**	

IOP PUBLISHING JOURNAL OF PHYSICS D: APPLIED PHYSICS

J. Phys. D: Appl. Phys. **45** (2012) 495401 (8pp) doi:10.1088/0022-3727/45/49/495401

Vibrational and rotational CARS measurements of nitrogen in afterglow of streamer discharge in atmospheric pressure fuel/air mixtures

S J Pendleton[1], A Montello[2], C Carter[3], W Lempert[2] and M A Gundersen[1]

[1] Pulsed Power Research Group, University of Southern California, Los Angeles, CA 90089, USA
[2] Michael A. Chaszeyka Non-Equilibrium Thermodynamics Laboratory, The Ohio State University, Columbus, OH 43210, USA
[3] Air Force Research Laboratory, Wright-Patterson Air Force Base, OH 45433, USA

E-mail: spendlet@usc.edu

Received 17 August 2012, in final form 19 August 2012
Published 9 November 2012
Online at stacks.iop.org/JPhysD/45/495401

Abstract
The use of nonequilibrium plasma generated by nanosecond discharges to ignite fuel/air mixtures, known as transient plasma ignition (TPI), has been shown to effectively reduce ignition delay and improve engine performance relative to spark ignition for combustion engines. While this method is potentially useful for many engine applications, at present the underlying physics are poorly understood. This work uses coherent anti-Stokes Raman spectroscopy (CARS) to measure the rotational and vibrational excitation of nitrogen molecules in the discharge afterglow in a variety of fuel/air mixtures outside the limits of combustion in order to elucidate the thermal behaviour of TPI. The time evolution of relative populations of vibrationally excited states of nitrogen in the electronic ground state are reported for each gas mixture; it is shown that generation of these vibrationally excited states is inefficient during the discharge in air but that generation occurs at a high rate roughly 5 μs following the discharge; with the addition of fuels vibrationally excited states are observed during the discharge but an increase in population is still seen at 5 μs. Possible mechanisms for this behaviour are discussed. In addition, rotational temperature increases of at least 500 K are reported for all gas mixtures. The effect of this temperature increase on ignition, reaction rates, and thermal energy pathways are discussed.

(Some figures may appear in colour only in the online journal)

1. Introduction and background

The application to an electrode gap of a very short duration electrical pulse of much greater amplitude than the gas breakdown voltage results in streamer discharge. The use of these streamers for ignition in combustion engines, or transient plasma ignition (TPI), holds great promise for improving combustion engines. To date, TPI has been tested in a variety of different ignition regimes, including pulsed detonation engines (PDEs) and automobile engines, with experiments demonstrating TPI to decrease ignition delay, increase flame speed, allow ignition of leaner mixtures, and increase the rate of heat release in comparison to standard spark gap or arc ignition methods [1–4]. Decreased ignition delay and increased flame speed are essential for effective operation of PDEs, while increasing heat release and allowing ignition of leaner mixtures improves the efficiency and thus the fuel economy of automobile engines. Furthermore, the technology is well developed with mature pulse generation technology having been successfully implemented into test engines [4–6].

Lagging behind the implementation and characterization of TPI in engines, however, is a detailed understanding of how the technology enhances combustion. Although TPI was initially assumed to be a primarily volumetric

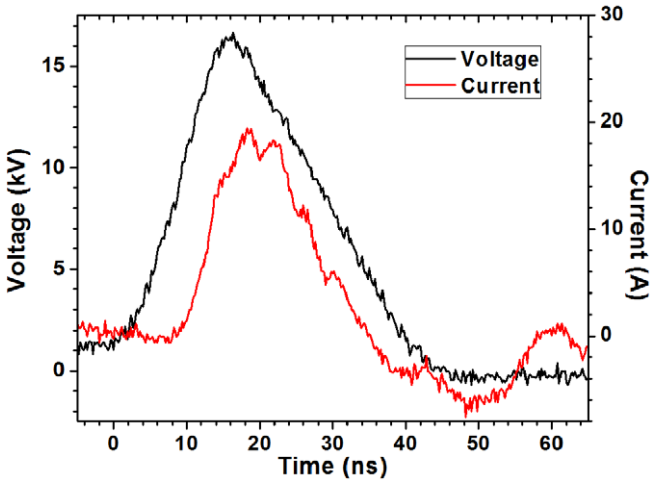

Figure 1. Voltage and current traces for the discharge in air.

effect, experimental work has shown TPI induces ignition in a spatially inhomogeneous manner, with combustion improvements independent from electrode volume [5, 7, 8]. The physics and chemistry of TPI are key to developing a predictive understanding of the technology and allowing engine design to fully utilize its potential to enhance combustion.

It is to this end that we here report coherent anti-Stokes Raman spectroscopy (CARS) measurements of vibrational populations and rotational temperatures of N_2 in the afterglow of streamer discharge in fuel/air mixtures outside the limits of combustion. These measurements elucidate energy transfer through the discharge as well as place upper limits on thermal energy deposition into the gas mixture.

2. Experiment

The experimental setup for these studies consists of a pulse generator and electrodes integrated into a flow-through pre-mixed gas system coupled to optical systems for conducting CARS and discharge emission imaging. A high voltage pulse generator nearly identical to that described in [5] was used for these experiments, with the silicon-controlled rectifier (SCR) replaced by a bank of commercial insulated-gate bipolar transistors (IGBTs) in parallel for the purposes of timing precision and repetition rate; the pulse-forming network was otherwise unchanged. This pulse generator produces a Gaussian-like voltage waveform (20 ns FWHM) with a controllable amplitude of 10–60 kV. Voltage and current traces of the discharge in air are shown in figure 1, with a Northstar PVM-5 voltage probe (80 MHz bandwidth) and a Pearson 6223 current probe used to record them on a LeCroy WavePro 725Zi oscilloscope. All data was recorded at a pulse repetition frequency of 10 Hz to match the optimal laser repetition rate.

TPI electrodes have traditionally used a coaxial design with a centre threaded rod high voltage anode and an outer grounded cathode due to the cylindrical symmetry inherent to most engine applications [1–3]. A fully three dimensional, multi-streamer electrode geometry, however, is problematic

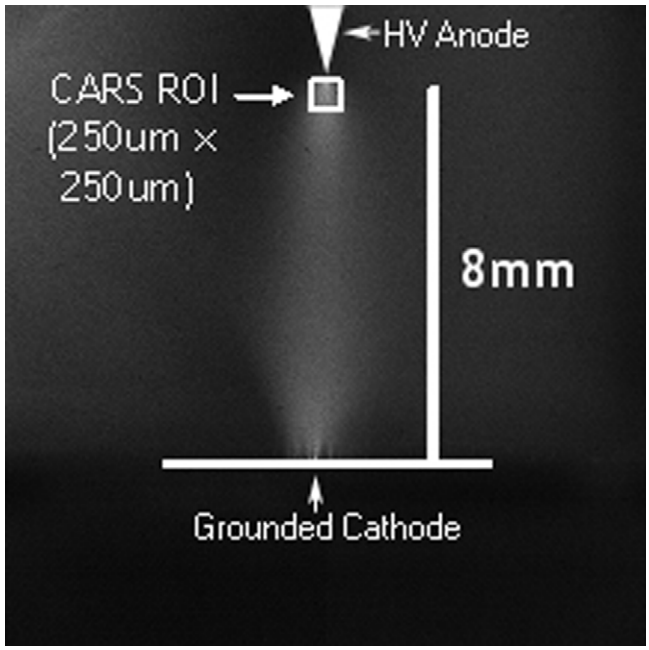

Figure 2. Image of discharge showing electrodes and spatial ROI, fitted around typical 250 μm streamer width near HV anode.

for laser-based diagnostics, especially for point measurements, and thus the electrodes were modified to a point-to-plane geometry for the purposes of these experiments, with a stainless steel needle with tip curvature of radius 75 μm as the high voltage anode and the sintered bronze surface of a McKenna burner (fabricated by Holthius and Associates) as the grounded cathode. Current was monitored using a Pearson 6223 current probe in line with the high voltage cable supplying the anode. The 8 mm gap used in previous TPI experiments was retained for the point-to-plane geometry. As previous experiments have demonstrated that ignition occurs in the region of high E/N near the anode, CARS measurements were made directly below the anode tip, as shown in figure 2 [8]. This region of interest (ROI) was chosen because the discharge was measured to be roughly 250 μm wide directly below the anode.

Gas compositions and flow rates were maintained with Tylan mass flow controllers. Flow rate was regulated to produce a gas speed of 10 cm s^{-1} to ensure complete recycling of gas volume in the discharge from shot to shot at 10 Hz while maintaining a quasi-quiescent environment. A McKenna burner with a sintered bronze circular burner of radius 3 cm was used to deliver a pre-mixed gas flow to the discharge region as well as serve as the grounded anode for the discharge; the needle anode was mounted 8 mm above the centre of the burner in order to isolate it from the edge of the flow and eliminate the need for a nitrogen co-flow. For all gas mixtures filtered facility compressed air was used to minimize moisture content. Ethylene (C_2H_4), methane (CH_4) and propane (C_3H_8), of purity 99.985%, 99.99% and 99.99%, respectively, were used for fuel/air mixtures. These fuels were chosen for comparison with previous TPI experiments [5–8]. The equivalence ratio of gas mixtures was chosen to be just outside of limits of flame stabilization for this system, with an extra point at half the lean

limit, in order to simulate the conditions of ignition without introducing the complication of unquenched combustion chain reactions and flame development. The fuel lean and rich limits were determined experimentally specifically for this setup.

Images of the discharge were taken using a Princeton Instruments PI-Max3 ICCD camera with a Nikon Nikkor 50 mm f/2.8 macro lens. The emission from the discharge is predominantly due to the nitrogen second positive system ($N_2(C\,^3\Pi_u) \rightarrow N_2(B\,^3\Pi_g)$), with the camera recording this emission in the range of 330–450 nm.

This work utilizes the unstable-resonator enhanced spatial detection (USED) CARS phase matching geometry [9]. While the spatial resolution of this approach (~2–3 mm) is less than that for folded BOXCARS, it is sufficient to achieve the objectives of this study, as will be described below. In the current arrangement, an Ekspla SL-333 Nd:YAG Laser, with maximum output of 125 mJ at 532 nm and pulse duration of ~150 ps, was used to generate the pump/probe beam for CARS mixing as well as pump the in-house fabricated modeless dye laser (patterned after Roy *et al* [10, 11]), which was used to generate the broadband Stokes beam. An Andor Shamrock 750 0.75 m spectrograph equipped with an Andor Newton electron multiplying CCD camera collected the CARS signal and non-resonant background. A more complete description of this setup may be found in [12]. For all CARS measurements reported, averages from 200 laser shots were used to increase the signal-to-noise ratio.

The time delay between the discharge and the laser was adjusted by triggering the system with a Stanford Research Systems DG-645 digital delay generator and varying the trigger delay between the laser and pulse generator. The delay was measured by simultaneously using a ThorLabs DET10A photodiode to collect laser scattering and monitoring the discharge current; the beginning of the current rise was specified as $t = 0$ for all work presented here. Every discharge event was probed by the laser only once as the heat deposition at such a high laser energy density would fundamentally alter the gas kinetics downstream in time; thus every time delay was measured in a separate discharge event and time sequences were constructed from the data in post processing rather than in real time.

The lasers were passed through the electrode gap directly beneath the anode. The position of the burner/electrode with respect to the laser beams was maintained with a three axis Newport MM300 motion controller/driver. The height of the beam with respect to the electrode was varied so that it could be as close to the electrode as possible without producing measurable scattering from the tip. The width of the beams passing through the discharge region are ~100 μm. In order to limit the signal generation to the discharge volume, the vibrational ground state of nitrogen was not used; only data from the excited vibrational states were taken into account, as these states are virtually nonexistent at room temperature. Thus, while the CARS probe region was ~2–3 mm in length along the propagation axis, only the 250 μm-wide volume of the discharge channel is taken into consideration, as only this region contains the excited vibrational states (though it is thus implicitly assumed that the temperature in probe region is uniform). The spectral ROI is shown in figure 3.

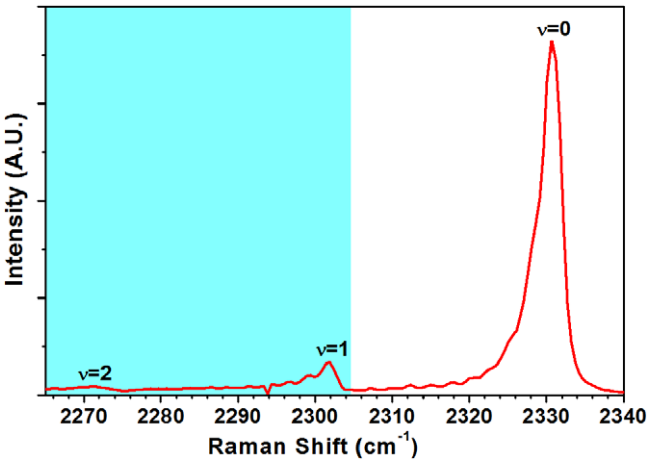

Figure 3. Raw CARS spectrum for air showing vibrational peaks. The shaded region is the spectral ROI.

The spectra, collected over 200 laser shots, must be divided by a non-resonant background spectrum measured in argon for each shot, to account for variation in the Stokes laser profile, and the square-root must be taken, to account for the quadratic dependence of CARS intensity on number density. After this, CARS spectra were analysed in two different ways. First, the signal for each ro-vibrational band was integrated over its spectral region in order obtain a relative population of vibrationally excited states with respect to time. Second, synthetic CARS spectra for each ro-vibrational band were calculated and least-squares fit to the measured spectra, with the rotational temperature as the fitting parameter. For each data point 200 spectra were fitted and the resulting temperatures were averaged together. As the measured CARS spectra contained etalons due to interference on the quartz walls of the laser dye cuvettes, the synthetic spectra also included a Fabry-Perot term as well as an empirically determined instrument broadening width of 1.4 cm^{-1}. Doppler and pressure broadening were determined to be negligible at these conditions compared to instrument broadening and were thus included in the instrument term. Generated and fitted spectra are shown in figure 4 for comparison. For this measurement at 200 μs delay, temperature was determined to fit best at 1000 $\pm$ 200 K with uncertainty determined by a combination of statistics based on the standard deviation of shot to shot variation and the quality of fit based on linear regression.

3. Results

Before optical measurements may be reported, it is necessary to fully characterize the discharge. Voltage and current traces were recorded and analysed for each gas mixture to quantify any changes in the electrode impedance. Despite noticeable macroscopic differences in different mixtures—the discharge pulses in richer mixtures were audibly louder than those in leaner mixtures for all three fuels—the measured electrical characteristics remained essentially identical with no more than 5% variation between any two mixtures in pulse width, peak current, peak voltage and energy delivered. Images

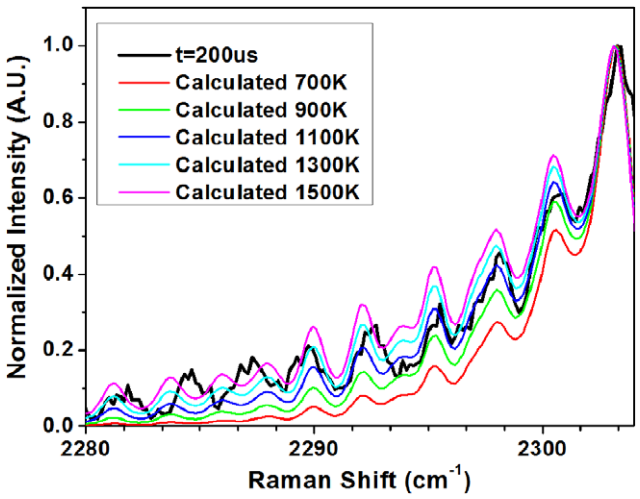

Figure 4. Measured (air) and calculated CARS spectra corresponding to 1000 K temperature fit.

were taken of the discharge in each mixture; in contrast to the relatively unaltered electrical input, the images bear out marked differences in streamer development with increased branching and decreased filament size with the addition of fuels as shown in figures 5–7. For example, for a rich mixture with a CH_4/air equivalence ratio of $\Phi = 1.2$, discharge branching has increased by a factor of roughly 10 with respect to air, similar to the increased branching observed in an equivalent discharge in pure nitrogen. The stability of the $\Phi = 1.2$ mixture with CH_4 was actually so poor that the addition of the CARS probe laser energy initiated breakdown and transition to arc and thus CARS was not performed for this mixture.

The results of CARS measurements in air for vibrationally excited $N_2(X\,^1\Sigma_g^+)$ are shown in figure 8. The $\nu = 1$ population is large enough to infer the temporal behaviour of this species. On the other hand the $\nu = 2$ signal, while observable, is too weak to extract accurate vibrational temperature, due to the very poor signal-to-noise ratio of this spectral feature. Typical minor fluctuations observed in the $\nu = 2$ intensity resulted in an inferred vibrational temperature range of thousands to tens of thousands of Kelvin for the conditions of this experiment. These deviations are too large to be physical; for this reason, we will report only the relative populations of $\nu = 1$ in fuel/air mixtures. Of note in air measurements is that the $\nu = 1$ signal is very weak until $\sim 2\,\mu$s after the discharge, indicating that vibrational excitation through direct electron impact in the discharge is negligible. This will be discussed at greater length below.

The $\nu = 1$ populations with C_2H_4/, CH_4/, and C_3H_8/air mixtures are shown in figures 9, 10 and 11, respectively. For the purposes of clarity uncertainty is shown only on a single point for each time sequence; the uncertainty displayed is the standard deviation of the mean taken from 200 shots and is comparable to that observed for all points in the given sequence. The $\Phi = 1.2$ mixture with CH_4 is omitted due to its instability under laser probing as previously mentioned. Like air the fuel/air mixtures exhibit an increase in $\nu = 1$ population at roughly $5\,\mu$s after the discharge, though the signal immediately after the discharge varies between fuel type.

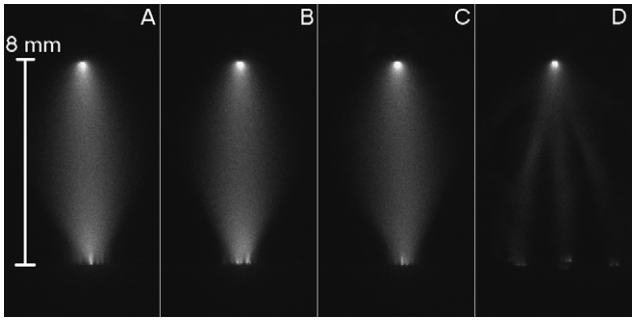

Figure 5. Images of the discharge in (*a*) air, $\Phi = 0$; (*b*) C_2H_4, $\Phi = 0.25$; (*c*) C_2H_4, $\Phi = 0.5$; (*d*) C_2H_4, $\Phi = 2.4$. The ICCD gate was 3 ns.

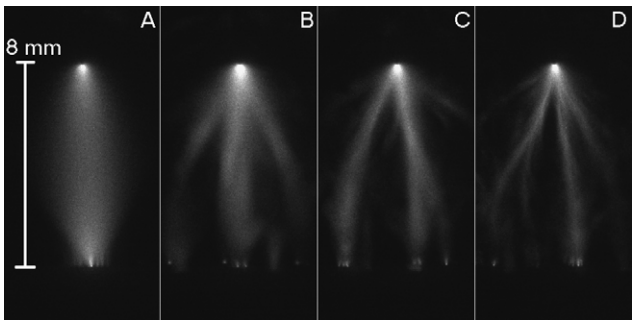

Figure 6. Images of the discharge in (*a*) air, $\Phi = 0$; (*b*) CH_4, $\Phi = 0.3$; (*c*) CH_4, $\Phi = 0.6$; (*d*) CH_4, $\Phi = 1.2$. The ICCD gate was 3 ns.

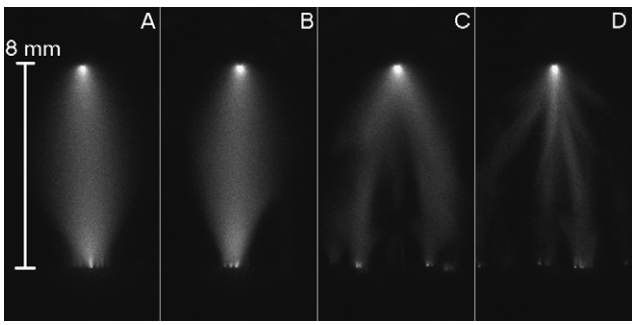

Figure 7. Images of the discharge in (*a*) air, $\Phi = 0$; (*b*) C_3H_8, $\Phi = 0.4$; (*c*) C_3H_8, $\Phi = 0.8$; (*d*) C_3H_8, $\Phi = 2.1$. The ICCD gate was 3 ns.

Where the $\nu = 1$ band displayed a signal-to-noise ratio of greater than unity, rotational temperatures were extracted; when this criterion was not met the uncertainty in temperature was greater than the fitted value. An example of this temporal overlap is shown in air in figure 12. The temperatures for C_2H_4/, CH_4/, and C_3H_8/air mixtures are shown in figures 13, 14 and 15, respectively. Note that the data points have been slightly offset from each other in time to avoid confusion from overlap, but they were measured at the same time points. As with the vibrational populations, uncertainty (here representing the standard deviation of the mean combined with least squares quality of fit) has been omitted except for a single point in each sequence for clarity, but the uncertainty plotted is comparable with that observed for the entire sequence.

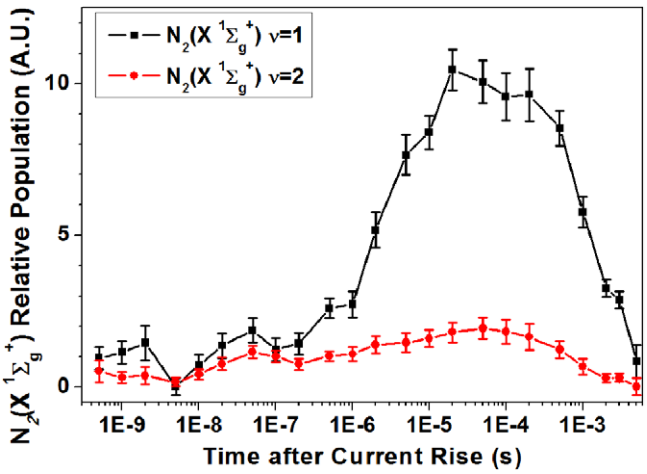

Figure 8. CARS measurements of vibrationally excited $N_2(X\,^1\Sigma_g^+)$ in air.

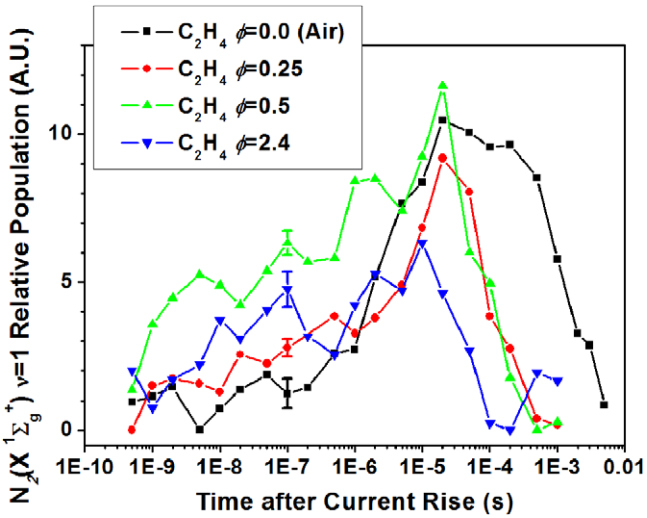

Figure 9. CARS measurements of vibrationally excited $N_2(X\,^1\Sigma_g^+)$ in C_2H_4/air mixtures.

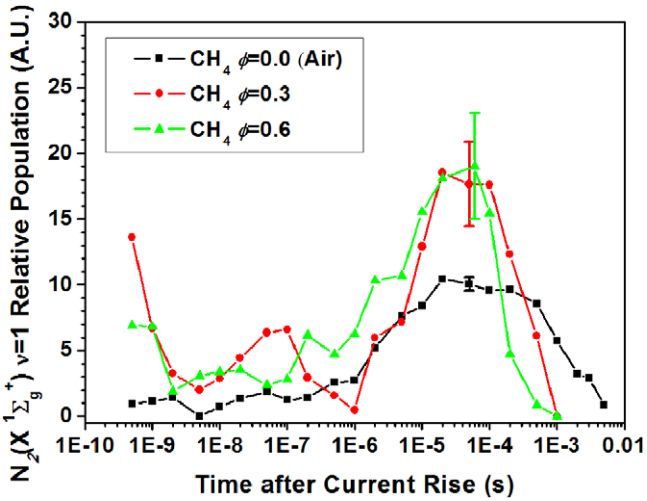

Figure 10. CARS measurements of vibrationally excited $N_2(X\,^1\Sigma_g^+)$ in CH_4/air mixtures.

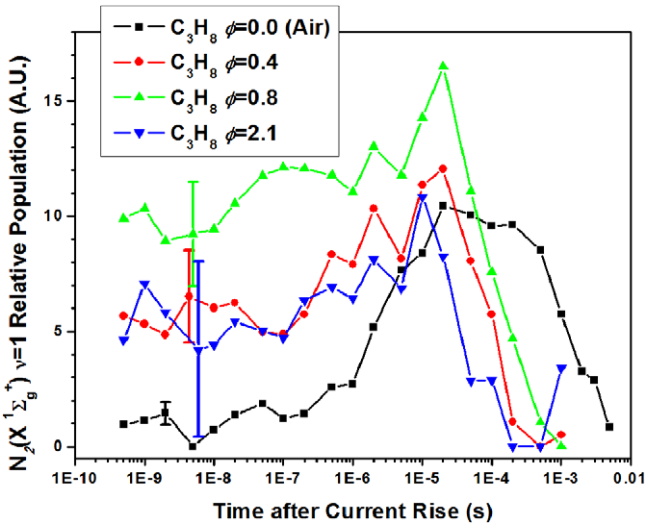

Figure 11. CARS measurements of vibrationally excited $N_2(X\,^1\Sigma_g^+)$ in C_3H_8/air mixtures.

4. Discussion

This work highlights the importance of optical diagnostics for TPI, especially for engine implementation. Based solely on electrical diagnostics of the discharge, gas composition has a negligible effect with energy input, voltage, and current all varying by less than 5%. This is reasonable as even with rich mixtures fuels comprise only 4–6% of the gas by mass and are not as active electrically in a discharge due to their relatively high ionization potential; thus, a great change in breakdown impedance is unexpected. Optical experiments bear out, however, that though the amount of energy deposited may remain fairly constant, the energy pathways differ greatly with small changes to the gas composition and that these changes depend on concentration as well as the chemistry of the introduced molecules.

Characterization of the discharge through ICCD imaging exhibits spatial and temporal changes resulting from the addition of fuel. Given enough of any fuel in the mixture the branching will increase and filament diameter will subsequently decrease (figures 5–7). CH_4/air mixtures exhibit this increased branching, however, with only a small amount of CH_4 in the gas. The same behaviour is seen in pure nitrogen discharges; somehow the fuels offset the effect of oxygen on the discharge front allowing multiple spatially distinct filaments.

When examining the CARS vibrational population data, the most striking result is the lack of measurable vibrationally excited $N_2(X\,^1\Sigma_g^+)$ during the discharge (i.e. within the time when current is nonzero or $t \leqslant 40$ ns for the present conditions) for air, signifying a vibrational temperature close to the ambient value (figure 8). This is in direct contrast to vibrational excitation of the $N_2(C\,^3\Pi_u)$ state, which exhibits high vibrational temperatures on the order of 3000 K during the discharge [13–15]. The delay in vibrational excitation of nitrogen corresponds to the flow moving only 100 nm downstream and the time scale of a few microseconds is too quick for such a large population to diffuse into the ROI; thus

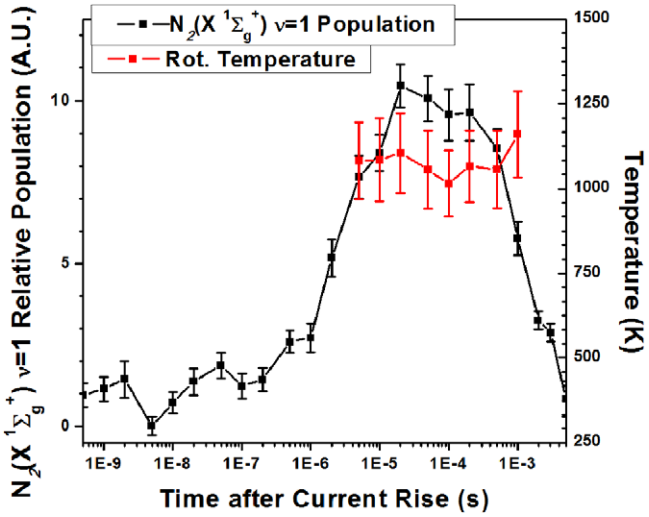

Figure 12. Rotational temperature overlaid with vibrational $v = 1$ signal in air showing required overlap between population and temperature extraction.

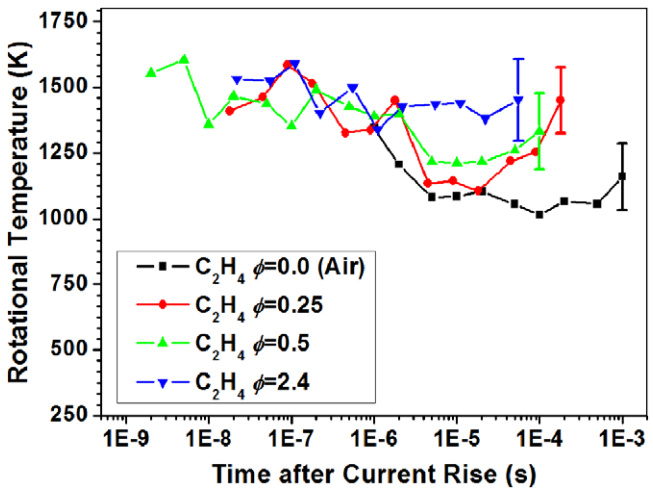

Figure 13. Rotational temperatures extracted from CARS for C_2H_4/air mixtures.

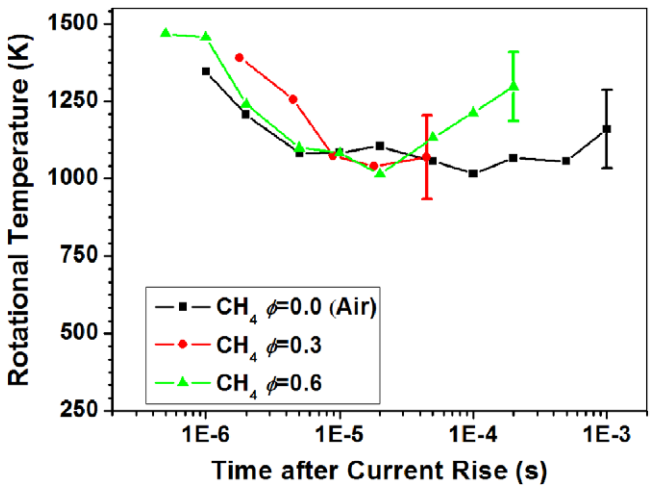

Figure 14. Rotational temperatures extracted from CARS for CH_4/air mixtures.

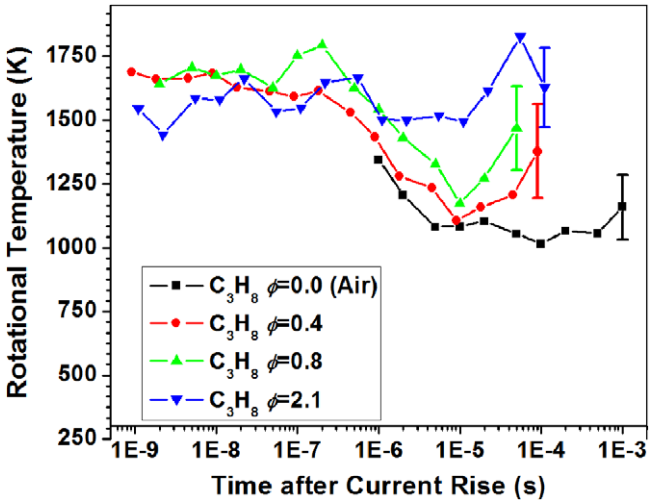

Figure 15. Rotational temperatures extracted from CARS for C_3H_8/air mixtures.

spatial anomalies may be ruled out as a cause of this behaviour. It is clear that in air direct vibrational excitation by electron impact is minimal, whereas vibronic excitation is relatively efficient by the same process. In the case of air, the eventual decay of the vibrational excitation signal at 2.5 ms corresponds with the initial discharge volume being completely displaced from the ROI by the gas flow, so conclusions about the vibrational lifetime cannot be made in air other than setting a minimum at 2.5 ms.

The addition of fuels alters this chemistry, but the change depends on the specific fuel (figures 9–11). Both C_2H_4/air and CH_4/air mixtures at all equivalence ratios display the presence of vibrationally excited nitrogen during the discharge and in the immediate afterglow, with CH_4/air mixtures showing an initial spike and quick decay within a few nanoseconds, though not to the levels of air at the equivalent time. In C_3H_8/air mixtures vibrational excitation is produced immediately in the discharge with no decay seen in the immediate afterglow; it is also particular to C_3H_8/air mixtures that the shot-to-shot variation of vibrational excitation is much greater than in other gas mixtures while the energy input variation remains low; the variational sensitivity is increased in C_3H_8/air along with the initial production of vibrational excitation. Of note is that none of these vibrational increases are monotonic with the increase of the amount of fuel in the mixture; the C_2H_4/air and C_3H_8/air mixtures exhibit the greatest change from pure air in the case where they are just below the lean limit of flame stabilization. The mixtures for these fuels above the rich limit exhibit behaviour closer to air, suggesting some sort of threshold effect on the facilitation by fuel molecules of direct electron impact vibrational excitation.

While the fuel/air mixtures exhibit different behaviour vis-à-vis nitrogen vibrational excitation in the discharge and immediate afterglow, they all exhibit an increase in $v = 1$ population at 1–10 μs of at least 50% in the case of rich C_3H_8/air mixtures and more than a 100% increase for all other mixtures. As this increase is consistent in time with pure air, this suggests that the rise of vibrationally excited nitrogen observed from 1–10 μs is due to collisional energy

transfer processes. Preliminary experiments in a pure nitrogen low pressure environment suggest that the effect is likely due to processes such as $N_2(A\,^3\Sigma) + N_2(A\,^3\Sigma) \rightarrow N_2(C\,^3\Pi) + N_2(X\,^1\Sigma, v)$ [16, 17]. In addition, recombination of atomic nitrogen could also contribute to the observed post-discharge increase in vibrational excitation, but for recombination to occur on this time scale would require ∼10% nitrogen dissociation in the discharge [18]. This rate of dissociation is highly unlikely given the low electron impact dissociation cross section below 15 eV; recent experiments measuring oxygen dissociation in this discharge cap the dissociation fraction for oxygen at 8% of molecules, and as the cross section for electron impact dissociation in this energy regime is roughly two orders of magnitude greater for oxygen than nitrogen, it is not possible for nitrogen to meet or exceed oxygen's dissociation rate [19, 20].

Another notable consistency across fuel/air mixtures is the decreased lifetime of vibrational excitation with respect to air, with the vibrational excitation disappearing by 1 ms. Flow displacement is ruled out as the mechanism for the signal decay, as the decay at this time is only observed in fuel/air mixtures, signifying that fuel molecules quench vibrational states of nitrogen at a rate that monotonically increases with concentration regardless of fuel type.

Rotational temperatures are observed to be significantly above ambient for all mixtures (figures 13–15). In pure air (no fuel) local rotational temperature reaches approximately 1100 K, corresponding to approximately 17 μJ of heat, or 0.4% of the discharge energy, being deposited into the ROI. If the ROI is extrapolated as a cylinder of diameter 250 μJ straight down from the anode along the 8 mm length of the discharge to the cathode, assuming a uniform temperature increase throughout this cylinder results in a total thermal energy deposition of the discharge of roughly 540 μJ, or 12% of the electrical pulse energy input. This is an upper bound on thermal energy input, as the energy input outside of the ROI must be less than that within the ROI due do a lower E/N away from the HV anode; this is evidenced by reduced emission intensity outside the ROI as well as the absence of ignition away from the electrode in combustion experiments [8].

In the case of CH_4/air mixtures, rotational temperature remains within 10% of pure air at the same time points, within the bounds of uncertainty. C_2H_4/air and C_3H_8/air mixtures experience significant increases with temperatures nearly 50% higher, seemingly independent of fuel concentration. For all fuel/air temperature data it appears that heat is generated immediately after the discharge and decreases monotonically on the microsecond-to-millisecond time scale, but does not reach ambient temperature before the gas is recycled with fresh unheated gas. The exponential decay time constant was fitted for each temperature sequence and ranged from 50 μs to 1.5 ms, with the mean falling at roughly 1 ms, corresponding to a temperature half life of 1.4 ms. In addition, the upper limit of thermal energy deposition for rich C_2H_4/air and C_3H_8/air mixtures, making the same assumptions as for air, is 840 μJ or 16% of total energy deposition into the discharge. This upper limit is most likely a greater overestimate than for the case of air, as the greater branching and thinner filament diameter in the discharge in rich fuel/air mixtures, as seen in figures 5–7, renders the assumption of constant streamer cross-sectional area void.

It is unlikely that electron impact would directly excite rotational levels in air given the relatively low excitation of vibrational levels by this process and the comparatively low cross section for the process [21]. Thus, the heat increase from air most likely comes from fast gas heating in the discharge afterglow due to incremental energy release in the decay and recombination of active species, with heating occurring sometime before 5 μs after the discharge based on measured temperatures. For the case of fuel/air mixtures, either direct electron impact excitation of rotational levels or ion recombination could account for such fast increases in temperature on the order of ns. Direct electron impact ro-vibrational excitation would be an immediate result of a lowering of the effective E/N to below 100 Td where such populating becomes more efficient, while ion recombination-based heating would require E/N on the order of 1000 Td or higher. It is much more likely that the presence of hydrocarbons draws energy from the discharge and thus effectively lowers E/N, given the low ion presence observed through emission spectroscopy in these discharges [14] as well as the presence of significant amounts of vibrational population, which is not a result of ion recombination.

The role of heat deposition in ignition of fuel/air mixtures by streamer discharge remains somewhat uncertain even in light of these temperature measurements. The estimates of the upper limit on thermal energy deposition into the discharge allow for ignition of C_2H_4 and C_3H_8 by the same thermal mechanisms seen in spark ignition; the estimated total 675 μJ of thermal energy deposition into both is well above the 100 μJ and 300 μJ minimum energy requirements for C_2H_4 and C_3H_8, respectively [22]. In the case of CH_4, the estimated 540 μJ is also greater than the 470 μJ minimum requirement reported for this fuel. Caution should be used when drawing the conclusion that streamers cause thermal ignition, however, as the estimates on the upper limits of thermal energy deposition required the assumption of temperature uniformity throughout the discharge as well as a cylindrical volume. In addition, the minimum energy requirements for spark ignition depend on a discharge volume that is within the quenching distance of a generated flame kernel (on the order of 1 mm for the fuels used in this work); the streamer discharge uses a much larger electrode gap. In order to bypass these assumptions and volume mismatches it makes sense to compare the energy densities of the two processes. In the case of CH_4, the deposited thermal energy density of the ROI measured in this work is 1080 mJ cm^{-3}, whereas the required deposited thermal energy density for spark ignition is 470 mJ cm^{-3}. For both C_2H_4 and C_3H_8, the measured deposited thermal energy densities are 1700 mJ cm^{-3}, well above the required thermal energy densities of 100 mJ cm^{-3} and 300 mJ cm^{-3} for C_2H_4 and C_3H_8, respectively. So while the thermal energy density is certainly high enough to ignite these fuel/air mixtures at stoichiometric conditions ($\Phi = 1$), it remains unclear whether the total deposited thermal energy is large enough to overcome thermal losses and produce a flame kernel that will expand beyond its

quenching radius. Further complicating the analysis are the effects of reactive species such as radicals that are produced in streamer discharge, which should allow ignition to occur with less total thermal energy input. These effects are not easily quantifiable based on available data.

5. Conclusion

The results of a comprehensive set of broadband picosecond coherent anti-Stokes Raman scattering measurements, describing the temporal evolution of vibrational and rotational excitation of N_2 in quasi-quiescent C_2H_4/air, CH_4/air, and C_3H_8/air mixtures outside the limits of combustion, were presented and analysed for a point-to-plane nanosecond streamer discharge similar to that used for transient plasma ignition. It was shown that direct electron impact vibrational excitation of nitrogen is relatively inefficient in this discharge in air, but in fuel/air mixtures electron impact accounts for roughly half of vibrational excitation of nitrogen. In all mixtures an intermediate process was demonstrated to generate vibrationally excited nitrogen at roughly 5 μs after the discharge, accounting for all vibrationally excited nitrogen in pure air and up to 50% of peak vibrationally excited nitrogen in fuel/air discharges; because this intermediate process occurs for both air and fuel/air mixtures, it is clear that the process results from the presence of nitrogen or oxygen or both. Further measurements in pure nitrogen could determine if the process depends on nitrogen or oxygen alone or some combination thereof. Temperature increases of 800 K in air and CH_4/air mixtures and 1300 K in C_2H_4/air and C_3H_8/air mixtures were observed; this corresponds respectively to upper limits of 10% and 16% of discharge energy deposited into thermal energy in a small region near the high voltage anode. These temperatures correspond to energy densities greater than the respective minimum value required for thermal ignition, but it remains unclear whether a sufficiently large volume is heated for purely thermal ignition to occur. Further experiments are necessary to quantify spatial temperature distribution as well as the production of reactive species such as oxygen atoms in order to better understand the physics and chemistry of TPI.

Acknowledgments

The authors would like to thank Igor Adamovich for discussions on chemical kinetics. They would also like to thank the Air Force Office of Scientific Research (Plasma Assisted Combustion MURI), the Propulsion Directorate's Summer Research Fellowship Program, the Office of Naval Research, NumerEx LLC and the National Science Foundation Graduate Research Fellowship Program for support.

References

[1] Cathey C D, Tao T, Shiraishi T, Urushihara T, Kuthi A and Gundersen M A 2007 Nanosecond plasma ignition for improved performance of an internal combustion engine *IEEE Trans. Plasma Sci.* **35** 1664–8

[2] Liu J, Wang F, Li G, Kuthi A, Gutmark E J, Ronney P D and Gundersen M A 2005 Transient plasma ignition *IEEE Trans. Plasma Sci.* **33** 326–7

[3] Wang F, Liu J B, Sinibaldi J, Brophy C, Kuthi A, Jiang C, Ronney P and Gundersen M A 2005 Transient plasma ignition of quiescent and flowing air/fuel mixtures *IEEE Trans. Plasma Sci.* **33** 844–9

[4] Shiraishi T *et al* 2009 A trial of ignition innovation of gasoline engine by nanosecond pulsed low temperature plasma ignition *J. Phys. D: Appl. Phys.* **42** 135208

[5] Singleton D R, Sinibaldi J O, Brophy C M, Kuthi A and Gundersen M A 2009 Compact pulsed-power system for transient plasma ignitio *IEEE Trans. Plasma Sci.* **37** 2275–9

[6] Singleton D R, Kuthi A, Sanders J M, Gundersen M A, Simone A and Pendleton S J 2011 Low energy compact power modulators for transient plasma ignition *IEEE Trans. Dielectr. Electr. Insul.* **18** 1084–90

[7] Cathey C, Cain J, Wang H, Gundersen M A, Carter C and Ryan M 2008 OH production by transient plasma and mechanism of flame ignition and propagation in quiescent methane-air mixtures *Combust. Flame* **154** 715–27

[8] Singleton D, Pendleton S J and Gundersen M A 2011 The role of non-thermal transient plasma for enhanced flame ignition in C_2H_4-air *J. Phys. D: Appl. Phys.* **44** 022001

[9] Marko K A and Rimai L 1979 Space- and time-resolved coherent anti-Stokes Raman spectroscopy for combustion diagnostics *Opt. Lett.* **4** 211

[10] Roy S, Meyer T R and Gord J R 2005 Time-resolved dynamics of resonant and nonresonant broadband picosecond coherent anti-Stokes Raman scattering signals *Appl. Phys. Lett.* **87** 264103

[11] Roy S, Meyer T R and Gord J R 2005 Broadband coherent anti-Stokes Raman scattering spectroscopy of nitrogen using a picosecond modeless dye laser *Opt. Lett.* **30** 3222–4

[12] Montello A, Nishihara M, Rich J W, Adamovich I V and Lempert W R 2012 Picosecond USED-CARS for simultaneous rotational/translational and vibrational temperature measurement of nitrogen in a nonequilibrium Mach 5 flow *50th AIAA Aerospace Sciences Meeting (Nashville, TN)* vol 2012

[13] Shcherbakov Y V and Sigmond R S 2007 Subnanosecond spectral diagnostics of streamer discharges: I. Basic experimental results *J. Phys. D: Appl. Phys.* **40** 460

[14] Pancheshnyi S, Sobakin S, Starikovskaya S and Starikovskii A 2000 Discharge dynamics and the production of active particles in a cathode-directed streamer *Plasma Phys. Rep.* **26** 1054–65

[15] Stancu G D, Kaddouri F, Lacoste D A and Laux C O 2010 Atmospheric pressure plasma diagnostics by OES, CRDS and TALIF *J. Phys. D: Appl. Phys.* **43** 124002

[16] Montello A, Yin Z, Burnette D, Adamovich I V and Lempert W R 2012 Picosecond CARS measurements of nitrogen vibrational loading and rotational/translational temperature in nonequilibrium discharges *43rd AIAA Plasmadynamics and Lasers Conf. (New Orleans, LA)* vol 2012

[17] Devyatov A A, Dolenko S A, Rakhimov A T, Rakhimova T V, Roi N N and Suetin N V 1986 Investigation of kinetic processes in molecular nitrogen by the CARS method *Sov. Phys.—JETP* **63**

[18] Ricard A, Tetreault J and Hubert J 1991 Nitrogen atom recombination in high pressure Ar-N2 flowing post-discharges *J. Phys. B: At. Mol. Opt. Phys.* **24** 1115–23

[19] Itikawa Y 2009 Cross sections for electron collisions with oxygen molecules *J. Phys. Chem. Ref. Data* **38** 1

[20] Itikawa Y 2005 Cross Sections for Electron Collisions with Nitrogen Molecules *J. Phys. Chem. Ref. Data* **35** 31

[21] Raju G G 2012 *Gaseous Electronics: Tables, Atoms, and Molecules* (Boca Raton, FL: CRC Press)

[22] Calcote H F, Gregory C A, Barnett C M and Gilmer R B 1952 Spark Ignition. Effect of Molecular structure *Indust. Eng. Chem.* **44** 2656–62